Sudhakar et al.

Lithium salts doped biodegradable gel polymer electrolytes for supercapacitor application

Y N Sudhakar[1], M Selvakumar[1*], D Krishna Bhat[2]

[1]*Department of Chemistry, Manipal Institute of Technology, Manipal, Karnataka, India.*
[2]*Department of Chemistry, National Institute of Technology Karnataka, Surathkal, Mangalore, India.*

*Corresponding Author. E-mail: chemselva78@gmail.com ; Tel; (+91 820-2571060)

Abstract
A biodegradable gel polymer (GPE) consisting of Xanthan gum (XG), glycerol, lithium salts like lithium perchlorate and lithium tetraborate were prepared. Using Fourier transform infrared spectroscopy (FTIR), thermal and scanning electron microscopy characterizations the interactions between the components in the gel matrix were studied. Furthermore, a unique electrochemical property was exhibited by GPEs as measured by AC impedance and dielectric studies. The role of anion in the enhancement of conductivity was important in the present study and highest conductivity of 6.4×10^{-2} S cm^{-1} at 333K was achieved among lithium salts. Supercapacitor was fabricated using GPE and tested for its electrochemical properties. Supercapacitor showed specific capacitance of was 82 Fg^{-1} at a scan rate of 5 mV s^{-1} for $Li_2B_4O_7$ and 74 Fg^{-1} at a scan rate of 5 mV s^{-1}. specific energy and specific power. Galvanostatic charge-discharge studies showed excellent cyclic stability.

Introduction

Gel formation techniques have become very popular in recent years, especially in the field of energy storage and biomedical sectors [1,2]. Gel polymer electrolytes (GPEs) employing poly (vinyl alcohol), poly (vinyl chloride), poly (ethylene oxide), poly (vinylidene carbonate) and poly (vinylidene fluoride) (PVdF) [1,3] etc., have shown better properties in concern to cost and stability. Biodegradable polymer electrolytes having good conductivity and stability were prepared to overcome the drawbacks of these petroleum derived polymers by few researchers [4-6]. Gums are classified under polysaccharide and are present in huge quantities in varieties of plants, animals, marine and microbial sources. Most of the gums available have tended to form gels upon addition of water and hence have gained vast application in various fields like oil drilling, food industries etc. Xanthan gum (XG) is a biopolymer with branched chains, obtained from the microbiological fermentation in aerobic conditions of sugar cane/corn, which is then transformed into a soluble gum during the reaction in the presence of the bacterium *Xanthomonas campestris*. XG is an acidic polymer consisting of pentasaccharide subunits, forming a cellulose backbone with trisaccharide side-chains composed of mannose (β-1,4) glucuronic acid, (β-1,2) mannose attached to alternate glucose residues in the backbone by α-1,3 linkages [7]. XG has excellent thermal stability in its solved state since it exhibits uniform viscosities over wide temperature ranges of freezing to near boiling. Even XG doped with acids, bases and salts have shown good solubility and stability. Due to these extraordinary properties XG is used in the food, cosmetic and pharmaceutical industries. Hence, XG was chosen as the gel polymer electrolyte for use in supercapacitor. Since XG is a highly branched polymer there is high possibility of intrahydrogen bondings, for that reason, glycerol was used as a plasticizer. Glycerol is a highly viscous solution and mainly used as plasticizers in natural polymers due to its retention among the polymer chains. With the optimized concentration of glycerol, it can break intra and inter hydrogen bonds of polymers, thereby certainly increasing the conductivity of the GPE.

Electrochemical double layer capacitor (EDLC) or supercapacitor is a device that stores energy more than conventional capacitors and offers short charging time, longer durability than batteries [8]. Lithium-polymer EDLCs are known to have slightly higher energy densities and reduced weight compared to lithium ion EDLC. In our previous work, an interaction between gel, LiClO$_4$ and plasticizer resulted in an unusual tubular array

which could be the cause of good energy density [9]. Therefore, in the present system two lithium salts having different anions were taken for better understanding of interactions in the gel system. Particularly, $LiClO_4$ has been chosen as a doping salt for its smaller size and highly electropositive characteristics even at low temperatures. $LiClO_4$ also has an advantage of less hygroscopic character and no formation of HF compared to other lithium salts like $LiBF_4$, $LiPF_6$ and $LiAsF_6$ [10]. Further, it may also be noted here that highly fluorinated compounds pose serious environmental concerns including that of biodegradation. The lithium tetraborate salt ($Li_2B_4O_7$) having an anionic group of higher affinity to OH group of polymer was also employed in this study. The fine structure of $Li_2B_4O_7$ would enhance the solubility in the polymer matrix and eventually, speed up the salt dissociation process. Other factors to choose $Li_2B_4O_7$ as a doping salt was due to its abundant availability of raw materials and no environmental pollution. Therefore, $Li_2B_4O_7$ is an indispensable electrolyte solute as it shows multiple merit than other lithium salts. Ramesh et al. [11] has used $Li_2B_4O_7$ as a dopant in a polymer which does not contains hydroxyl groups, yet a conductivity of ~10^{-6} S cm^{-1} was obtained. In view of the fact that both $LiClO_4$ and $Li_2B_4O_7$ can be used as dopants, our interest is to compare these salts interactions with abundantly containing OH group polymer in a gel matrix.

In view of the aforesaid aspects, we report the fabrication of a supercapacitor employing a novel GPE system based on biodegradable and renewable polymer. XG was doped with $LiClO_4$ and $Li_2B_4O_7$ and glycerol was used as plasticizer. GPEs having the highest ionic conductivity were chosen for FTIR, thermal and scanning electron microscopic characterizations. Furthermore, at different temperatures, ionic conductivities, dielectric constant and dielectric loss as well as the real and imaginary parts of the electrical modulus were analyzed for GPEs. Supercapacitor performance was evaluated employing AC impedance spectroscopy, cyclic voltammetry (CV) and galvanostatic charge-discharge (GCD) techniques. Based on the highest specific capacitance, the EDLC was further chosen for cyclic performance studies.

2. Materials and methods
2.1. GPE preparation
XG (medium molecular weight) and glycerol were purchased from Merck. Lithium perchlorate (Aldrich) and lithium tetraborate (Loba Chemi) were dried at 393K and kept under vacuum for 48 h before use. 1 wt% of XG stock solution were prepared in distilled water. Appropriate amount of stock solution, plasticizer and salts were mixed as given in Table. 1, wherein A series presents $LiClO_4$ doped GPE and S series presents $Li_2B_4O_7$ doped GPE. The ratio of stock solution to plasticizer was optimized to maintain the jelly character of good strength. The prepared solutions were placed in clean 10 ml beakers separately and allowed to bring about gelation initially at room temperature and were then kept in a water bath at 333K for 48 h to form GPEs before subjecting to other studies.

Table 1: Gel contents

Sample	Polymer solution(wt%)	Plasticizer (wt%)	Salt (wt%)
A1	80	20	0.015
A2	80	20	0.020
A3	80	20	0.025
S1	80	20	0.020
S2	80	20	0.025
S3	80	20	0.030

2.2. Characterisation
FTIR measurements of the pure XG and Li salt doped XG samples were carried out at room temperature using Shimadzu FTIR 8460S (Japan). Thermogravimetric analysis (TGA)/Differential thermal analysis (DTA) measurements were done using DTA-60 Model instruments from Shimadzu. Measurements were done over a temperature range of 303K and 473K at a heating rate of 10 °C min^{-1} under the nitrogen atmosphere at flow rate of 60 mg l^{-1} and readings were taken from the first heating run.

The solid GPE samples were cut into small cubes and freeze dried in a deep freezer. Later, freeze dried samples were kept in a nitrogen atmosphere and then subjected to high vacuum. The micro images were taken using a scanning electron microscope (SEM), ZEISS EVO 18 special edition.

2.3. Conductivity and electrochemical studies

For electrochemical studies, samples having thickness of ~2 mm were cut into 1×1 cm^2 dimensions and placed between two square stainless steel electrodes (length 1 cm) fitted with copper wires. The whole set up was holded tightly with a plastic clamp. The bulk ionic conductivities (σ) and dielectric properties of the blends were determined from the AC impedance in the frequency range between 1 MHz and 100 mHz using a small amplitude AC signal of 10 mV. Experiments were carried out in the temperature range of 303K and 333K. The formulae and relationships between complex impedance, dielectric permittivity and dielectric modulus can be found elsewhere [6].

2.4. Fabrication of supercapacitor cell

Electrode material for supercapacitor fabrication was prepared using activated carbon (AC) [12]. AC was coated on two stainless steel electrodes using PVdF as a binder. The supercapacitor cell was constructed using GPE sandwiched between two AC coated electrodes. Electrochemical characterization was carried out using CV, AC impedance, and GCD studies. All the electrochemical characterization was carried out using Biologic SP-150 instrument.

3. Results and Discussion
3.1. Ionic conductivity studies

In Fig. 1, as temperature increased, there was an increase in the conductivity of the GPEs since the polymer chains acquires faster internal modes of vibration in which bond rotations produce segmental motion, favouring inter-chain and intra-chain lithium ion hopping movements on the oxygen atom of XG [13].
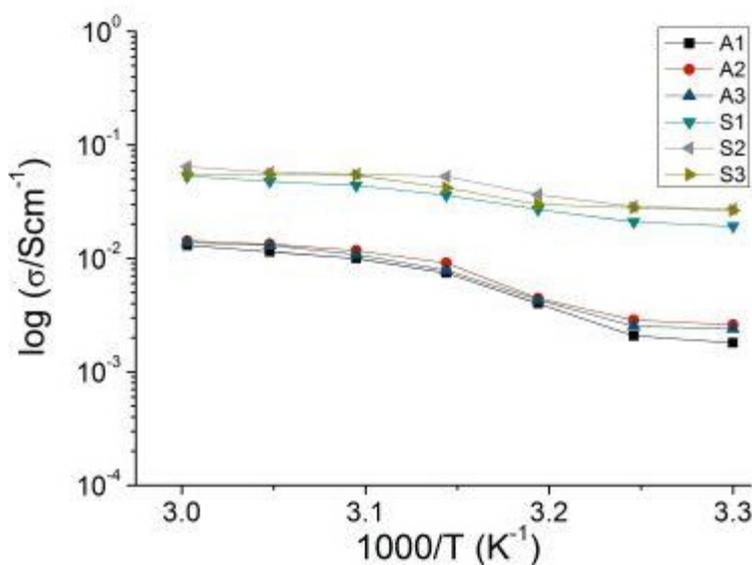
Figure 1: Variations of bulk conductivities of GPEs with different temperatures.

Ionic conductivity was calculated from complex impedance spectra using the equation $\sigma_0 = L/RA$, where *L*, *R* and *A* are the thickness, bulk resistance and area of the GPE, respectively. The highest ionic conductivity was exhibited by the sample S2, i.e., 6.4×10^{-2} S cm^{-1} at 333K and 2.7×10^{-2} S cm^{-1} at 303K. Whilst, the ionic conductivity of LiClO$_4$ doped GPE (A2) was 1.4×10^{-2} S cm^{-1} at 333K and 2.6×10^{-3} S cm^{-1} at 303K. In a view point, A1 has shown lower ionic conductivities since the low concentration of LiClO$_4$ could not effectively break the intermolecular bonding between XG chains. Later, decrease in ionic conductivity was observed to increase in salt concentration in both the Li doped systems because the ionic motion was hindered within the gel matrix and only the plasticizer retained in the gel matrix helped in the conduction of ions. Noor et al. [14] reported gellan gum-lithium trifluoromethane sulfonate based GPE showing 5.4×10^{-4} S cm^{-1} conductivity,

which is less than present system. Present work conductivity was found to be greater than other natural polymers like gellan gum, cellulose, chitosan, starch, agar and pectin [9,15]. The conductivity-temperature relationship of the GPE obeys Arrhenius behaviour, and activation energy can be calculated from the relation $\sigma=\sigma_0 \exp(-E_A/kT)$, where σ_0 is the pre-exponential factor, E_A is activation energy, k is the Boltzmann constant, and T is absolute temperature. The values of E_A for GPEs studied in this work were in the range of 0.20–0.34 eV for $Li_2B_4O_7$ doped GPE and 0.51-0.64 eV for $LiClO_4$ doped GPE. The electrolyte with lower value of E_A implies that dopant salt has been dissociated favouring ionic conduction by forming coordination with other polymer sites. The increase in E_A with an increase in salt indicates the formation of ion pairs or aggregates and hence decreasing the conductivity.

The bulk resistance was calculated from the high-frequency intercept of semicircle on the real impedance axis of the Nyquist plot as a function of temperature for samples S2 and A2. As shown in Figs. 2a and b, the bulk resistance of the GPE at higher frequencies decreases with increase in temperature in both S2 and A2, respectively. At low frequency region, initially at 303K a vertical response was observed, which is characteristic of ideal response. This might be due to the presence of many ions near the electrode/electrolyte interface containing plasticizer rich region. At 333K, the bulk resistance decreased drastically leading to random orientations of dipoles in the side chains and even rupturing of weak hydrogen bonding between glycerol and XG. Further, the reduction in the vertical line of Warburg impedance suggests that there is an increase in the liquid component of the gel system. Comparatively, the bulk resistance of $Li_2B_4O_7$ doped GPE was less than $LiClO_4$ doped GPE in studying temperatures, indicating increased Li ion diffusion that might be because of increased dissociation of $Li_2B_4O_7$ than $LiClO_4$ in XG/glycerol system.
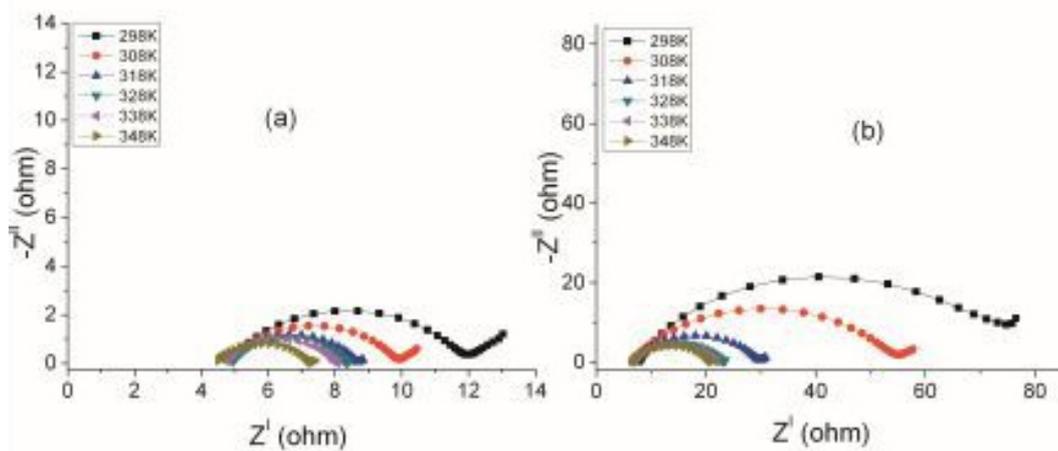
Figure 2: Nyquist plots of the GPEs at different temperatures (a) S2 and (b) A2.

3.2. Dielectric studies

The variation of dielectric constant (ϵ_R), dielectric loss (ϵ_I), real part of the electric modulus (M_R) and imaginary part of the electric modulus (M_I) at 303K for GPE samples A2 and S2 are shown in Figs. 3 and 4, respectively. ϵ_R and ϵ_I spectra of both A2 and S2 show the values rising sharply in the low frequency region and decaying at high frequency region. As frequency increases, the ϵ_R decreases because of the high periodic reversal of the electric field at the interface, which reduces the contribution of charge carriers towards the dielectric constant [16]. As the temperature increased the values decreased slowly indicating the stability of the ions at electrode/electrolyte interface region. Comparatively, the dielectric values of $Li_2B_4O_7$ doped GPE are 10 times more than $LiClO_4$ doped GPE, indicating greater number of free Li^+ ions in the A2 gel matrix. Thus, the increase in mobile ions increased the conductivity in view of the fact that the conductivity is proportional to the number of mobile ions.

The peaks of the modulus formalism at high frequencies show that the present GPE is ionic conductor. A tail was observed in the lower part of frequency, which indicates the sample is capacitive in nature. The presence of relaxation peaks in M_R and M_I of $LiClO_4$ doped GPE indicates that residual water contribute towards conductivity enhancement [17]. Consequently, it may be suggested that the charges causing these effects are closely associated with the gel itself, rather than exist in a free state within the network in $Li_2B_4O_7$ doped GPE. The peak curve at higher frequencies may be due to the bulk effect that mechanism will be discussed later.
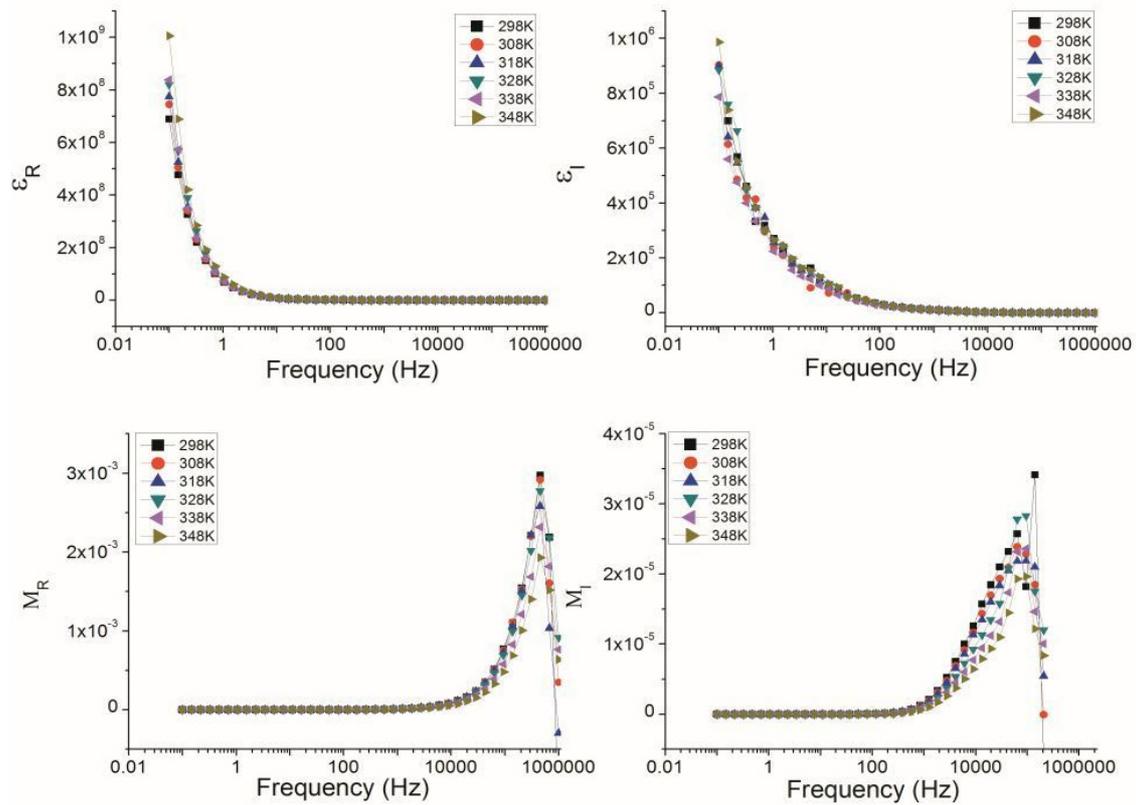
Figure 3. Plots of dielectric studies versus frequency at different temperatures (a) dielectric constant, (b) dielectric loss, (c) real part of electric modulus, and (d) imaginary part of electric modulus of A2.

3.3. FTIR studies

Fig. 5 show FTIR spectra of pure XG, A2 and S2. The spectra display the main characteristic peaks of polysaccharides in the range of 900-1100 cm^{-1}.
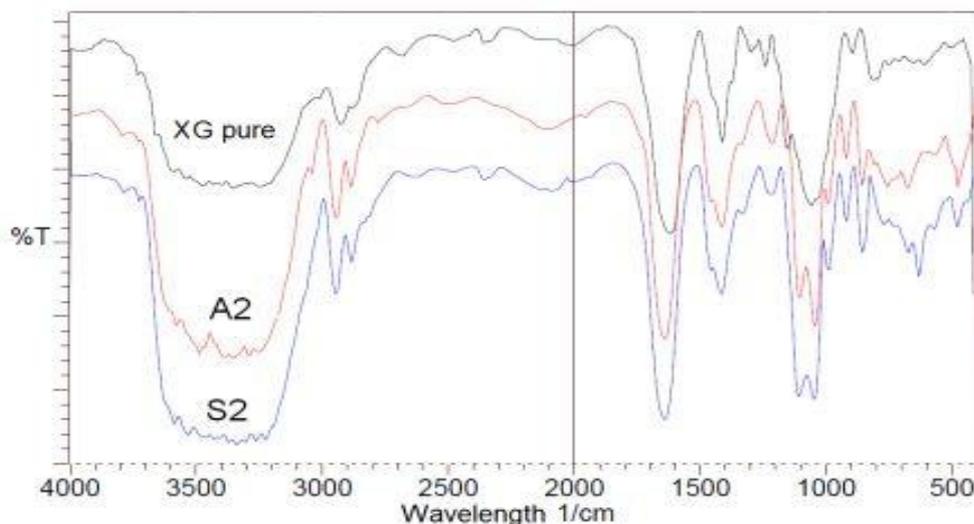
Figure 5: FTIR spectra of pure XG, S2 and A2.

The peaks at 1026–1056 cm^{-1} are characteristic of the anhydroglucose ring. The peak at 1411 cm^{-1} is due to OH bending. The large peak at 1620 cm^{-1} are due to the bound water present in the xanthan gum. The band of 2885–2923 cm^{-1} is characteristic of C–H stretching. A broadband due to hydrogen bonded hydroxyl group (O–H) appeared in 3420–3434 cm^{-1} and is attributed to the complex vibrational stretching, associated with free, inter and intra molecular bound hydroxyl groups [18]. Upon addition of lithium salts these

characteristic peaks shifted to higher wave numbers indicating their interaction with the gel matrix, while the peak of the solvent at 1411 cm^{-1} is undisturbed further confirming that the interaction is between the lithium salt ions and the polymer chains. Comparatively, the Li$^+$ peak at 630 cm^{-1} in S2 exists more intensely than A2, indicating more free ions are present in S2 sample. Even shift of 1620 cm^{-1} peak to 1643 cm^{-1} in S2 indicates an increased interaction between salt and polymer rather than water.

3.4. TGA/DTA studies

TGA was performed for pure XG, A2 and S2 (Fig. 6). In pure XG, the initial weight loss that began at 100 °C is due to the presence of a small amount of moisture in the sample. The second degradation region is at 302 °C, wherein the polymer decomposition starts and continues up to 422 °C [19]. For plasticized LiClO$_4$ doped system, onset of degradation temperature after evaporation of water is 228 °C and end set is 259 °C. Whilst, for Li$_2$B$_4$O$_7$ doped GPE onset of degradation temperature after evaporation of water is 234 °C and end set is 262 °C. Thus, it can be concluded from TGA results that plasticizer and doping of salt have significantly affected the thermal stability of the GPE system in comparison with pure XG. Moreover, Li$_2$B$_4$O$_7$ doped GPE exhibits more stability compared to the LiClO$_4$ doped system. This also supports the results derived from the FTIR data that there is more interaction between polymer and Li$_2$B$_4$O$_7$ than LiClO$_4$.
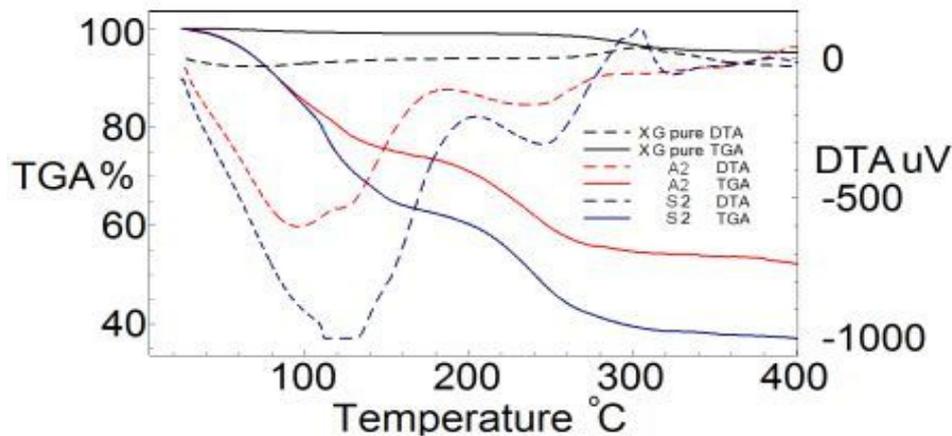
Figure 6: TGA and DTA measurements of pure XG, S2 and A2.

3.5. SEM analysis

Figs. 7a and b are SEM images of A2 and S2 samples, respectively. In Fig. 7a rough surface indicate the existence of crystal domains due to few undissociated LiClO$_4$. Fig. 7b shows a smooth surface due to the dual compatibility of XG towards glycerol which tends to lessen the driving force for the separation and leads to better development of the gel. The interaction produced a additional relaxed network in the matrix. The absence of several pores or craters on the surface indicates no rapid evaporation of the solvent (water).
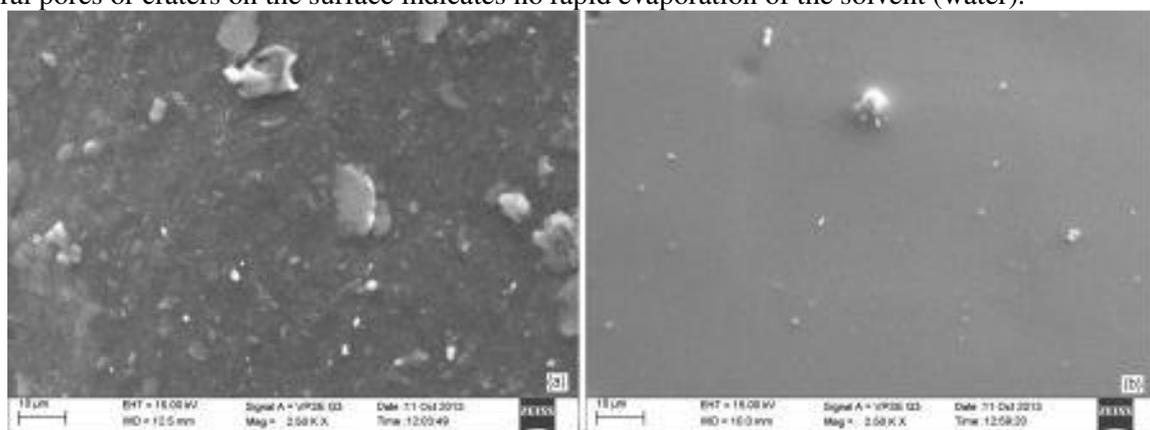
Figure 7: SEM images of (a) A2 and (b) S2.

3.6. Predicted interaction mechanism

Based on the evidence obtained from characterization studies, the interaction of polymer, glycerol and lithium salts is predicted in Figs. 8a and b. Fig. 8a show interaction of $Li_2B_4O_7$ doped GPE, wherein the Li^+ and tetraborate anions formed are well dissociated in the gel matrix due to hydrogen bonding between tetraborate anions and hydroxyl groups [11] of XG. This interactions of XG segments and anions make the gel stable at varying temperature. This provides a well-directed pathway of Li^+ ions to transport along the specified channels of plasticizer in the gel matrix. Fig. 8b show interaction of $LiClO_4$ doped GPE wherein poor dissociation occurs because only Li^+ ions are activly involved in bonding with OH groups of XG and hence polymer segments are dispersed in plasticizer, thereby leaving behind ionic aggregates at certain regions in the gel matrix. Since ionic conductivity is measured majorly by cationic movement in the polymer electrolyte, the $LiClO_4$ doped GPE has a less ionic conductivity than $Li_2B_4O_7$ doped GPE. High conductivity might also be due to the presence two Li^+ in tetraborate salt, whereas there is only one Li^+ bounded with perchlorate anion. Hence, the role of anion was important in the enhancement of ionic conductivity.
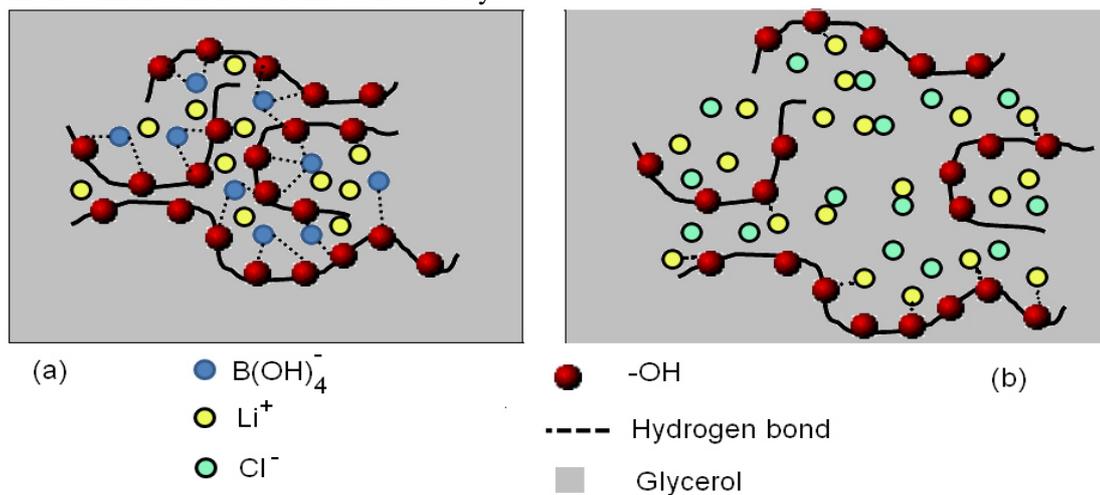
Figure 8: Predicated mechanism of ionic conduction in GPEs (a) $Li_2B_4O_7$ doped GPE and (b) $LiClO_4$ doped GPE

3.7. Supercapacitor studies

GPE with higher conductivity A2 and S2 were used to construct two separate supercapacitors. CV responses for the carbon–carbon symmetrical supercapacitor at various sweep rates are shown in Fig. 9a and b for A2 and S2, respectively.
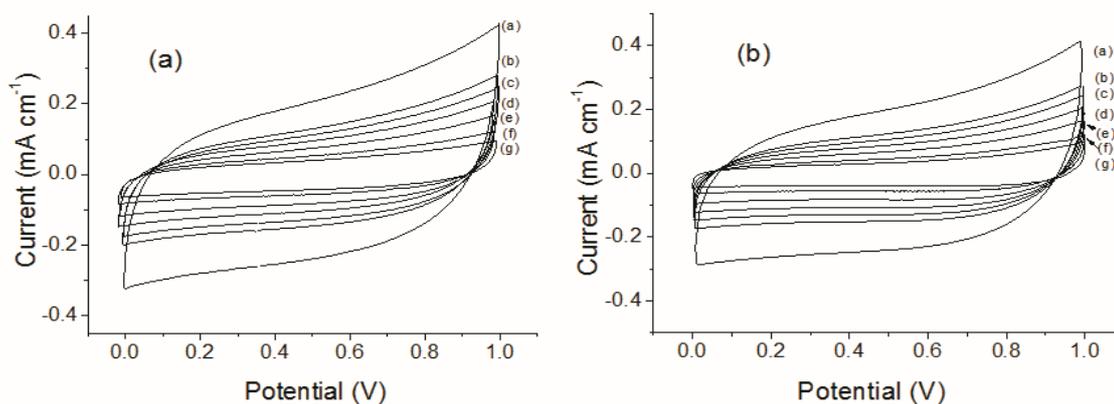
Figure 9a and b: CVs of EDLC containing A2 and S2 supercapacitors, respectively at (a) 50 mV s^{-1}, (b) 25 mV s^{-1}, (c) 20 mV s^{-1}, (d) 15 mV s^{-1} (e) 10 mV s^{-1}, (f) 5 mV s^{-1}, and (g) 2 mV s^{-1}

Calculations of specific capacitance, specific power (P), specific energy (E) and equivalent series resistance (ESR) were obtained from the literature [20]. The specific capacitance values of the SC has been calculated from the respective cyclic voltammograms using the equation;

$$C = \frac{2\Delta I}{\Delta V \times m} \qquad (1)$$

where ΔV is the voltage scan rate, m is the mass per electrode. ΔI the average current and C the specific capacitance. Using charge/discharge studies, discharge capacitance (C_d) was calculated using equation

$$C_d = \frac{I \times \Delta t}{\Delta V \times m} \qquad (2)$$

$$E = \frac{C_d \times \Delta V^2}{2} \times \frac{1000}{3600} \qquad (3)$$

$$P = \frac{I \times \Delta V}{2 \times m} \times 1000 \qquad (4)$$

$$ESR = \frac{IR_{drop}}{2 \times I} \qquad (5)$$

where I (A) is the discharge current, Δt (s) is the discharge time, m (g) is the weight of active material, ΔV (V) represents the voltage change after a full charge or discharge, and IR drop (V) is the electrical potential difference between the two ends of a conducting phase during charging/discharging. A maximum specific capacitance of LiClO$_4$ doped supercapacitor was 74 Fg^{-1} at a scan rate of 5 mV s^{-1} and for Li$_2$B$_4$O$_7$ doped supercapacitor was 82 Fg^{-1} at a scan rate of 5 mV s^{-1}. The specific capacitance values were greater than other biodegradable elelctrolyte based supercapacitor [21] and comparable to that of Choudhury et al. [22]. This implies that a large amount of mobile Li$^+$ is available in the Li$_2$B$_4$O$_7$ doped supercapacitor, which leads to a high capacitance of the device. The CV curve rectangular features indicates the capacitive behaviour of the supercapacitor, i.e., double layer formation at the interfaces [23].

AC impedance was measured to investigate the change of the resistance of the components and the formation of a double layer at electrode/electrolyte interface region. Figs. 10a and b show AC impedance response of supercapacitor fabricated using activated carbon and GPEs. In Fig. 10a, Nyquist plot at lower frequency region has R_{ct} value of 0.8 Ω for LiClO$_4$ doped supercapacitor and Fig. 10b has R_{ct} value of 0.6 Ω for Li$_2$B$_4$O$_7$ doped supercapacitor. This indicates that there is less availability of Li$^+$ ions in LiClO$_4$ doped system to form a double layer at the electrode/electrolyte interface [24]. From Fig. 10 (inset) the calculated time constant was found to be equal to (i) 0.3 s for LiClO$_4$ doped supercapacitor and (ii) 0.2 s for Li$_2$B$_4$O$_7$ doped supercapacitor.
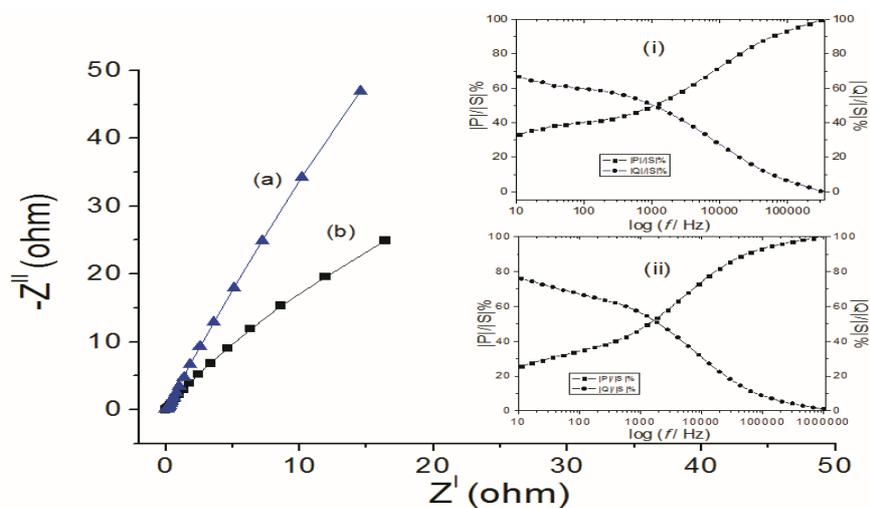
Figure 10: AC impedance plots of (a) A2 and (b) S2 supercapacitors [inset: Plots of normalized reactive power |Q|/|S|% and active power |P|/|S|% versus frequency (Hz) of (i) A2 and (ii) S2].

Galvanostatic charge/discharge measurements were performed to study the influence of the ionic conductivity on the performance of the constant current charge and discharge characteristics of the supercapacitors. Figs. 11a (A2) and b (S2) show the charge/discharge profile of the supercapacitors as measured by the galvanostatic method by varying current densities of 0.25 mA cm^{-2}, 0.5 mA cm^{-2} and 1 mA cm^{-2} between potential window of 1 V. All curve profiles clearly indicate typical capacitor behaviour.
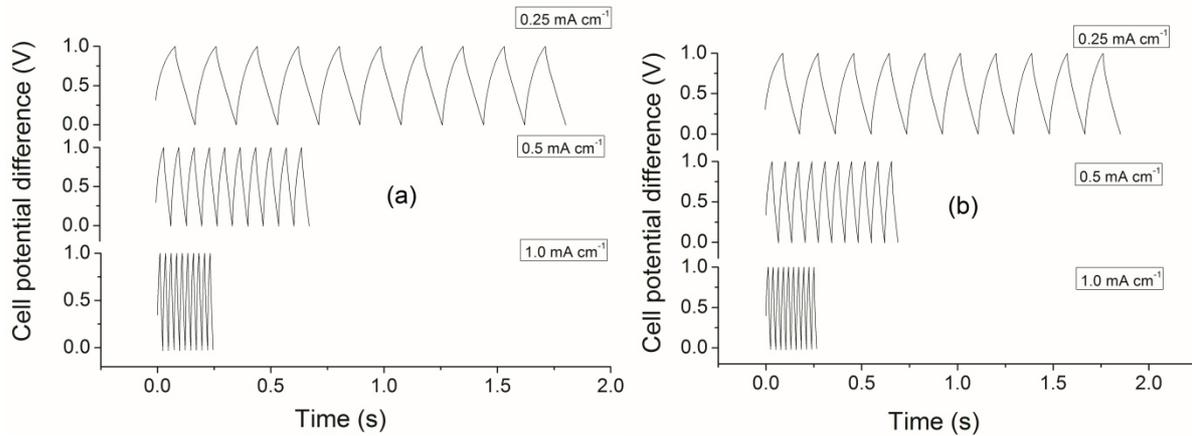
Figure 11a and b: Galvanostatic charge/discharge plots for A2 and S2 supercapacitors at different current densities, respectively.

Furthermore, the GCD stability of GPE was measured at a constant current density of 1 mA cm^{-2} between potential widow of 1 V, i.e., between 0 V and 1.0 V up to 2000 cycles (Fig. 12).
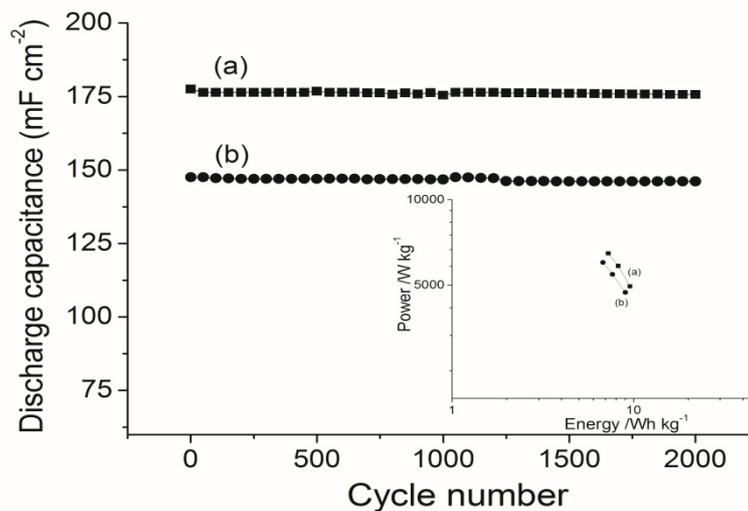
Figure 12: Discharge capacitance versus number of cycles and Ragone plot (inset) of (a) S2 and (b) A2. (Current density: 1 mA cm^{-2})

The initial decrease in the capacitance values is minimum, which is due to the loss of the charges initially stored at interface associated with the irreversible reactions of loosely bound surface groups on the porous activated carbon electrodes [6]. Specific energy (SE) values ranged between 6.7 Wh kg^{-1} and 9.0 Wh kg^{-1} for LiClO$_4$ doped supercapacitor, and 7.2 Wh kg^{-1} and 9.5 Wh kg^{-1} for Li$_2$B$_4$O$_7$ doped supercapacitor. Specific power (SP) values ranged between 4700 W kg^{-1} and 6000 W kg^{-1} for LiClO$_4$ doped supercapacitor, and 4900 W kg^{-1} and 6500 W kg^{-1} for Li$_2$B$_4$O$_7$ doped supercapacitor as observed in the Ragone plot (Fig. 12, inset). Comparatively, the specific energy was less than value reported in literature [20], but this system showed higher specific power. Specific power was found to be similar to redox based KOH-m-phenylenediamine supercapacitor [25]. This shows the improved interaction of ions at the electrode/electrolyte interface which readily leads to double layer. Table 2 shows calculated values discharge capacitance, Columbic efficiency, ESR and IR drop. It will be very interesting in performing further research by incorporating high performance electrodes, in order to achieve high capacitance, stability, thin and flexible supercapacitors that can substitute electrolytic capacitors.

Table 2: Values calculated from charge/discharge curves

	Discharge capacitance	Columbic efficiency	ESR	IR drop
$Li_2B_4O_7$ doped supercapacitor	168 mF cm^{-1}	97%	62	0.03 V
$LiClO_4$ doped supercapacitor	147 mF cm^{-1}	96%	84	0.04 V

Conclusions

In summary, we have reported comparison between $LiClO_4$ and $Li_2B_4O_7$ doped GPEs, wherein good interaction was observed in $Li_2B_4O_7$ doped GPE. The highest ionic conductivity was exhibited by the sample S2, i.e., 6.4×10^{-2} S cm^{-1} at 333K and 2.7×10^{-2} S cm^{-1} at 303K. Better dissociation property of the GPE system was evident in $Li_2B_4O_7$ doped GPE as observed in FTIR and thermal studies. This studies showed a unique behaviour of increased conductivity due to anionic interaction with the polymer by providing a pathway to the transport of cations towards the electrode. The dielectric studies indicated the high capacitive nature and supported the structure of gel matrix. A fabricated carbon–carbon supercapacitor showed a specific capacitance of 74 F g^{-1} at a scan rate of 5 mV s^{-1} for $LiClO_4$ doped GPE, and 82 F g^{-1} at a scan rate of 5 mV s^{-1} for $Li_2B_4O_7$ doped GPE. The supercapacitor showed good specific power and specific energy and was quite stable during charge/discharge cycles with high columbic efficiency. Finally, this work suggests that even biodegradable gel polymer electrolytes from renewable sources can be efficiently used in high energy and power storage devices.

References

1. Baskakova Y. V., Efimov O. N., *Russ. Chem. Rev.* 81 (2012) 367.
2. Ha C. S., Gardella J. A., *Chem. Rev.* 105 (2005) 4205.
3. Senthilkumar S. T., Selvan R. K., Ponpandian N., Melo J. S., *RSC Advances*, 2 (2012) 8937.
4. Choudhury N. A., Northrop P. W. C., Crothers A. C., Shruti J., Subramanian V., *J. Appl. Electrochem.* 42 (2012) 935.
5. Vieira D. F., Avellaneda C. O., Pawlicka A., *Electrochim. Acta*, 53 (2007) 1404.
6. Sudhakar Y. N., Selvakumar M., *Electrochim. Acta*, 78 (2012) 398.
7. Darioa A. F., Hortencioa L., Sierakowskib M. R., Netoc J. C. Q., Petri D. F. S., *Carbohydr. Polym.* 84 (2011) 669.
8. Zhang L., Zhao X., *Chem. Soc. Rev.* 38 (2009) 2520.
9. Sudhakar Y. N., Selvakumar M., Bhat D. K., *Mat. Sci. Engineering B* 180 (2014) 12.
10. Zhang M., Dahn J. R., *J. Electrochem. Soc.* 143 (1996) 2730.
11. Ramesh S., Chao L. Z., *Ionics*, 17 (2011) 29.
12. Natalia M., Sudhakar Y. N., Selvakumar M., *Indian J. Chem. Technol.* 20 (2013) 392.
13. Reddy S. C. V., Sharma A. K., Narasimha V. V. R., *J. Power Sources* 114 (2003) 338.
14. Noor I. S. M., Majid S. R., Arof A. K., Djurado D., Claro N. S., Pawlicka A., *Solid State Ionics*, 225 (2012) 649.
15. Varshney P. K., Gupta S., *Ionics* 17 (2011) 479.
16. Rajendran S., Prabhu M. R., *J. Appl. Electrochem.* 40 (2010) 327.
17. Ahmad Z., Isa M. I. N., *Int. J. Latest Res. Sci. Technol.* 1 (2012) 70.
18. Shalviri A., Liu Q., Abdekhodaie M. J., Wu X. Y., *Carbohydr. Polym.* 79 (2010) 898.
19. Pandey S. Mishra S. B., *Int. J. Biol. Macromol.* 49 (2011) 527.
20. Yu H., Wu J., Fan L., Lin Y., Xu K., Tang Z., Cheng C., Tang S., Lin J., Huang M., Lan M., *J. Power Sources* 198 (2012) 402.
21. Selvakumar M, Bhat D. K., Physica B 404 (2009) 1143.
22. Choudhury N. A., Sampath S., Shukla A. K., *J. Electrochem. Soc.* 155 (2008) A74.
23. Rikukawa M., Sanui K., *Prog. Polym. Sci.* 25 (2000) 1463.
24. Tambelli C. E., Donoso J. P., Magon C. J., Pereira E. C., Rosario A. V., *Electrochim. Acta*, 53 (2007) 1535.
25. Yu H., Fan L., Wu J., Lin Y., Huang M., Lin J., Lan Z., *RSC Advances*, 2 (2012) 6736.